

On the primordial origin of the smoothing excess in the *Planck* temperature power spectrum in light of LSS data

Mario Ballardini,^{1,2,3,4,5,6} Fabio Finelli^{4,5}

¹Dipartimento di Fisica e Scienze della Terra, Università degli Studi di Ferrara, via Giuseppe Saragat 1, I-44122 Ferrara, Italy

²INFN, Sezione di Ferrara, via Giuseppe Saragat 1, I-44122 Ferrara, Italy

³Dipartimento di Fisica e Astronomia, Alma Mater Studiorum Università di Bologna, via Gobetti 93/2, I-40129 Bologna, Italy

⁴INAF/OAS Bologna, via Piero Gobetti 101, I-40129 Bologna, Italy

⁵INFN, Sezione di Bologna, via Irnerio 46, I-40126 Bologna, Italy

⁶Department of Physics & Astronomy, University of the Western Cape, Cape Town 7535, South Africa

E-mail: mario.ballardini@unife.it, fabio.finelli@inaf.it

Abstract. The *Planck* DR3 measurements of the temperature and polarization anisotropies power spectra of the cosmic microwave background (CMB) show an excess of smoothing of the acoustic peaks with respect to Λ CDM, often quantified by a phenomenological parameter A_L . A specific feature superimposed to the primordial power spectrum has been suggested as a physical solution for this smoothing excess. Here, we investigate the impact of this specific localized oscillation with a frequency linear in the wavenumber, designed to mimic the smoothing of CMB temperature spectrum corresponding to $A_L \simeq 1.1 - 1.2$ on the matter power spectrum. We verify the goodness of the predictions in perturbation theory at next-to-leading order with a set of N-body simulations, a necessary step to study the non-linear damping of these primordial oscillations. We show that for a large portion of the parameter space, the amplitude of this primordial oscillation can be strongly damped on the observed non-linear matter power spectrum at $z = 0$, but a larger signal is still persistent at $z \lesssim 2$ and is therefore a target for future galaxy surveys at high redshifts. From an analysis of the BOSS DR12 two-point correlation function, we find $\mathcal{A}_{\text{lin}} < 0.26$ at 95% CL by keeping the frequency fixed to the best-fit of *Planck* data.

Contents

1	Introduction	1
2	Primordial oscillatory features with a Gaussian envelope	2
3	Cosmological simulations with primordial features	5
4	Perturbation theory with primordial features	5
4.1	Comparison with cosmological simulations	8
5	Comparison with current LSS data	10
6	Conclusions	12

1 Introduction

An excess of smoothing in the region of the acoustic peaks of the CMB anisotropy temperature power spectrum has been found in all three *Planck* data releases [1–3]. This effect is often quantified by a phenomenological parameter A_L which scales the theoretical prediction for the lensing contribution. The excess from $A_L = 1$ (the prediction of general relativity) represents one of the current intriguing discrepancies within *Planck* data plaguing the standard Λ CDM model [4–6].

Results from the *Planck* Collaboration based on DR3 correspond to $A_L = 1.180 \pm 0.065$ (2.8σ) using the baseline `Planck` likelihood [3, 7] and using the `CamSpec` likelihood $A_L = 1.149 \pm 0.072$ (2.1σ) [3, 8] both at 68% CL combining low- ℓ and high- ℓ temperature and polarization data when CMB lensing information is not included (see Ref. [9] for an early indication for higher lensing contribution from the combination of WMAP 3Y and ACBAR CMB data). Latest results based on the `CamSpec` likelihood with *Planck* DR4 also show an excess, $A_L = 1.095 \pm 0.056$, although at a lower significance (1.7σ) mainly due to differences in EE and TE [10]. Current results from CMB ground-base telescope are more consistent with Λ CDM predictions: $A_L = 1.01 \pm 0.11$ with ACT DR4 [11] and $A_L = 0.98 \pm 0.12$ with SPT-3G 2018 EE/TE data [12]. By folding in *Planck* CMB lensing data the estimate of A_L decreases to smaller values [13].

The residuals between *Planck* data and the Λ CDM best-fit yield an oscillatory pattern, which can be mimicked by a specific localized oscillations superimposed to the primordial power spectrum (PPS), see Refs. [14–18].¹ It has been recently shown that with this type of primordial feature, a higher value for H_0 and a smaller value of S_8 than in Λ CDM can be simultaneously found [17, 18].

¹Note that the degeneracy between the effect of lensing on the CMB temperature power spectrum and oscillating primordial feature was already pointed out in Ref. [19].

However, oscillations in the PPS cannot mimic A_L in all the different CMB fields at the same time because the peaks in CMB polarization are out of phase with those in temperature [15]. Indeed, the phase of the E-mode polarization peaks follows the velocity fluid making the turning points of temperature peaks corresponding to zero points of velocity (this implies a $\pi/2$ shift in phase). In addition, the correlation power spectrum TE, being the product of the two, exhibits acoustic peaks with twice the acoustic frequency. Moreover, matter and radiation oscillations are not in phase implying a $\pi/2$ shift in phase between Fourier mode connected to the decoupling of photons and baryon [20]. These differences point to the possibility to use future CMB polarization and/or large-scale structure (LSS) clustering measurements in order to further test the primordial origin of the CMB smoothing excess.

LSS clustering information has been highlighted as an excellent observable to test primordial oscillations on small scales and for high frequencies as shown in many forecast studies in Refs. [21–28] and demonstrated on real data in Refs. [27, 29, 30]. Indeed, the case of primordial features with linear and logarithmic oscillations have been workhorses for the studies with perturbation theory [27, 28, 31–34] and N-body simulations [28, 31, 33, 34] in order to have accurate theoretical predictions for LSS clustering observables.

Indeed, Fig. 1 shows that current measurements of the matter power spectrum (for a compilation of inferences of the linear matter power spectrum at redshift $z = 0$ following the method proposed in Refs. [38, 39]) are potentially able to put some constraint on this specific template considering the best-fit amplitude and the location of the feature of one of the primordial feature model proposed in order to recover $A_L \simeq 1$ in Ref. [15].

In this paper, we extensively study the imprint on the matter power spectrum of a localized primordial oscillation with a frequency proportional to k proposed in Ref. [15]. In Sec. 2, we introduce the model studied and we describe the comparison between its pattern and the lensing contribution on the CMB spectra and the baryon acoustic oscillations (BAO) signal on the matter power spectrum. We describe and show the results from our simulations in Sec. 3 and we compare them to the predictions from perturbation theory in Sec. 4. Finally, we derive the constraint on the feature amplitude using the two-point correlation function from BOSS DR12 in 5. Sec. 6 contains our conclusions.

2 Primordial oscillatory features with a Gaussian envelope

As show in [14, 15], the effects of the phenomenological lensing parameter A_L can be mimicked by injecting in the PPS a feature oscillating linearly in k with a frequency and a phase matching to the one of the acoustic peaks of the CMB angular power spectra. In particular, it is fundamental that the oscillations have a scale-dependent modulation in order to reproduce $A_L \simeq 1$. We study the following template with damped linear oscillations

$$\mathcal{P}_{\mathcal{R}}(k) = \mathcal{P}_{\mathcal{R},0}(k) \left[1 + \mathcal{A}_{\text{lin}} e^{-\frac{(k-\mu_{\text{env}})^2}{2\sigma_{\text{env}}^2}} \cos \left(\omega_{\text{lin}} \frac{k}{k_*} + \phi_{\text{lin}} \right) \right]. \quad (2.1)$$

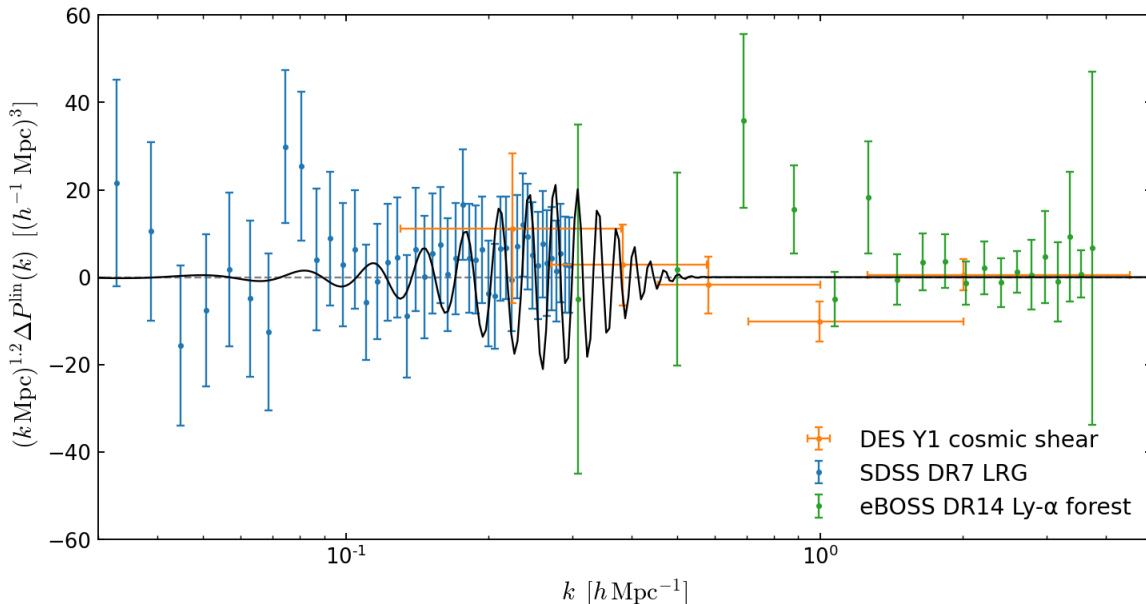


Figure 1. Figure comparing measurements [35–37] and linear theoretical predictions adapted from Ref. [38].

where $\mathcal{P}_{\mathcal{R},0}(k) = A_s (k/k_*)^{n_s-1}$ is the standard power-law PPS of the comoving curvature perturbations \mathcal{R} . A_s and n_s are the amplitude and the spectral index of the comoving curvature perturbations at a given pivot scale $k_* = 0.05 \text{ Mpc}^{-1}$. Because of the dependence of the template on five parameters and the degeneracy among them, the parameters for which the template mimics the effect A_L are not uniquely determined. We will consider as examples for the parameters to mimic $A_L \simeq 1$ those quoted in [15]: $\mathcal{A}_{\text{lin}} = 0.16$, $\omega_{\text{lin}} = 10^{1.158} \simeq 14.4$, $\mu_{\text{env}} = 0.2 \text{ Mpc}^{-1}$, $\sigma_{\text{env}} = 0.057 \text{ Mpc}^{-1}$, and $\phi_{\text{lin}} = \pi$. This choice is not however important for our considerations and there might other choices of parameters which also show the degeneracy of the template in Eq. (2.1) with $A_L \simeq 1$.

This particular template matches reasonably well the residuals between the CMB temperature angular power spectrum and the ΛCDM bestfit, but does not reproduce the residuals in polarization and temperature-polarization cross-correlation, as already emphasized in [15]. In Fig. 2, we show the comparison between the feature best-fit and the featureless power spectrum with $A_L = 1.18$. While Eq. (2.1) with the best-fit parameters above can recover the residuals for the case with $A_L = 1.18$ for the CMB temperature, it does not for the E-mode polarization and the temperature-polarization cross spectra unless we change both the frequency and the phase.

In Fig. 3, we compare the template with damped linear oscillations with BAO feature at redshift $z = 0$. The two signals have different frequency, phase and they peak at different wave-number.

Finally, the CMB lensing power spectrum is not very sensitive to this class of primordial features with high frequencies [40]. The power spectrum of the lensing potential is an integrated quantity where a large range of wavenumbers contribute to

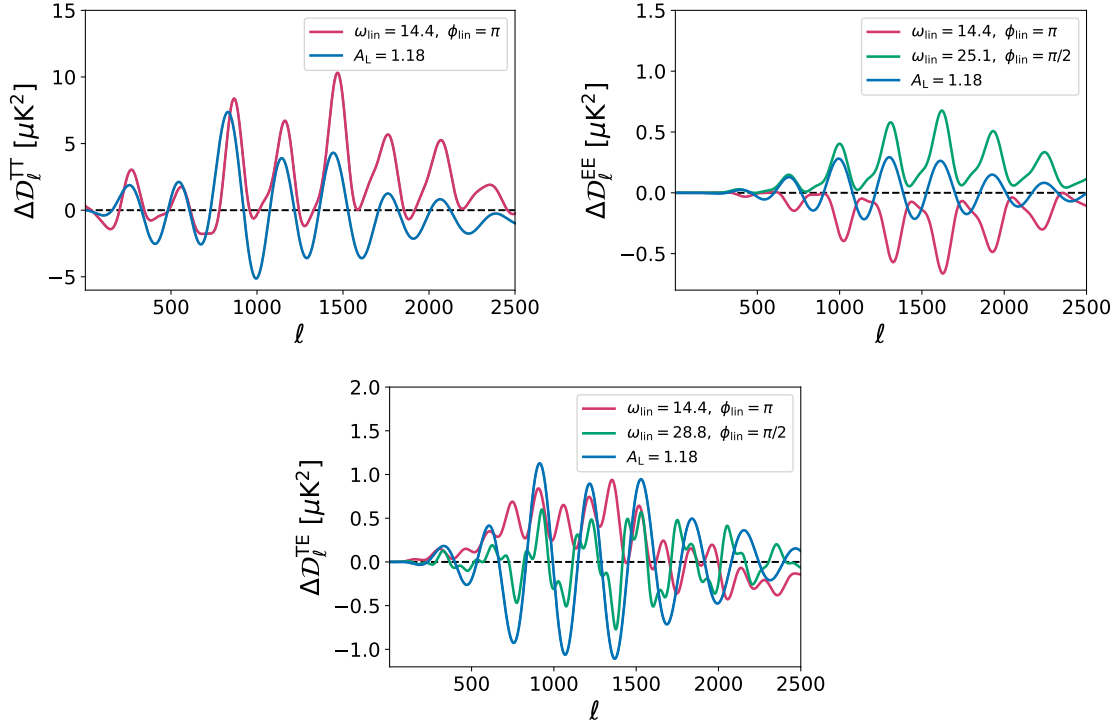


Figure 2. Differences with respect to the Λ CDM CMB angular power spectrum for the case with $A_L = 1.18$ (blue) and for the features template (2.1).

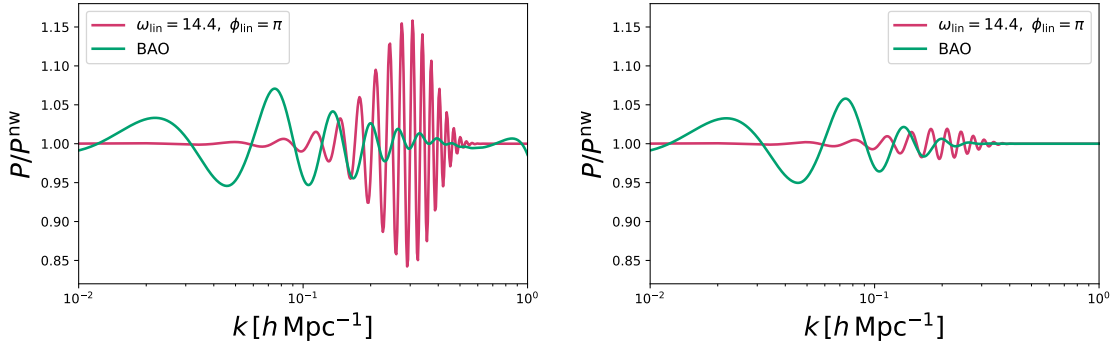


Figure 3. Comparison between the BAO signal (green line) and the template (2.1) with $A_{\text{lin}} = 0.16$, $\log_{10} \omega_{\text{lin}} = 1.158$, $\phi_{\text{lin}} = \pi$ (magenta line). *Left panel:* ratio of the linear matter power spectrum at $z = 0$. *Right panel:* ratio of the non-linear matter power spectrum at $z = 0$.

each multipole; as a result, high frequency oscillations as those considered here are efficiently smoothed in CMB lensing compared to CMB temperature and polarization spectra.

3 Cosmological simulations with primordial features

In order to study the effect of such signal imprinted on the matter power spectrum, we have run a modified version of the publicly available code L-PICOLA² [41–43] to produce a total of nine simulations with different cosmological parameters. We have fixed the standard cosmological parameters to $h = 0.6736$, $\Omega_m = 0.31377$, $\Omega_b = 0.04930$, and $\sigma_8 = 0.8107$ according to Ref. [3]. Initially, we start with the fiducial feature parameters described in [15] (hereafter M1) and the corresponding featureless case. Subsequently, we have studied the effect of varying one of the feature parameters at the time: M2 with $\mathcal{A}_{\text{lin}} \rightarrow \mathcal{A}_{\text{lin}}/2 = 0.08$, M3 with $\mathcal{A}_{\text{lin}} \rightarrow 2\mathcal{A}_{\text{lin}} = 0.32$, M4 with $\mu_{\text{env}} \rightarrow \mu_{\text{env}}/2 = 0.1 \text{ Mpc}^{-1}$, M5 with $\mu_{\text{env}} \rightarrow 2\mu_{\text{env}} = 0.4 \text{ Mpc}^{-1}$, M6 with $\sigma_{\text{env}} \rightarrow \sigma_{\text{env}}/2 = 0.0285 \text{ Mpc}^{-1}$, M7 with $\sigma_{\text{env}} \rightarrow 2\sigma_{\text{env}} = 0.114 \text{ Mpc}^{-1}$, M8 with $\log_{10} \omega_{\text{lin}} \rightarrow 0.8 \log_{10} \omega_{\text{lin}} = 0.926$, and M9 with $\log_{10} \omega_{\text{lin}} \rightarrow 1.2 \log_{10} \omega_{\text{lin}} = 1.39$.

Each simulation has 1024^3 dark matter particles with a comoving box with side length of $1024 h^{-1} \text{ Mpc}$ evolved with 30 time steps³. The initial conditions are produced using second-order Lagrangian Perturbation Theory, with the 2LPTic code [44], at redshift $z = 9$, with input the linear matter power spectra were computed with a modified version of the publicly available code CAMB⁴ [45], as in [28].

In order to minimize cosmic variance, we run pair of simulations with the same initial seed, inverted initial condition, and with fixed amplitude as in [28]. Finally, we use observable averaged over these two simulations. Using paired-fixed simulations, with paired phase [46, 47] and fixed amplitude [46, 48], significantly reduces the variance of the N-body simulations; see Ref. [49] for a comprehensive study of this procedure.

In Fig. 4, we show the relative differences between the nonlinear matter power spectrum of the feature model (2.1) with respect to the featureless case for the feature bestfit and the eight models (from the top to the bottom) at different redshift $z = 0, 1, 2$ (from the left to the right).

4 Perturbation theory with primordial features

Following the perturbative approach in Refs. [27, 32], closely connected to the BAO resummation done in [50, 51], we start by decomposing the linear power spectrum into a smooth (nw) and an oscillating (w) contribution

$$P^{\text{lin}}(z, k) = G^2(z) [P^{\text{nw}}(k) + P^{\text{w}}(k)] . \quad (4.1)$$

Here the oscillatory part describes both BAO and the primordial oscillations as

$$P^{\text{w}}(k) \equiv P^{\text{nw}} [\delta P_{\text{BAO}}^{\text{w}}(k) + \delta P_{\text{lin}}^{\text{w}}(k) + \delta P_{\text{BAO}}^{\text{w}}(k) \delta P_{\text{lin}}^{\text{w}}(k)] \quad (4.2)$$

with

$$\delta P_{\text{lin}}^{\text{w}}(k) = \mathcal{A}_{\text{lin}} e^{-\frac{(k-\mu_{\text{env}})^2}{2\sigma_{\text{env}}^2}} \cos\left(\omega_{\text{lin}} \frac{k}{k_*} + \phi_{\text{lin}}\right) \quad (4.3)$$

²<https://github.com/CullanHowlett/l-picola>

³We found consistent and robust results by running smaller simulations with 512^3 particles and a box with side of $512 h^{-1} \text{ Mpc}$.

⁴<https://github.com/cmbant/CAMB>

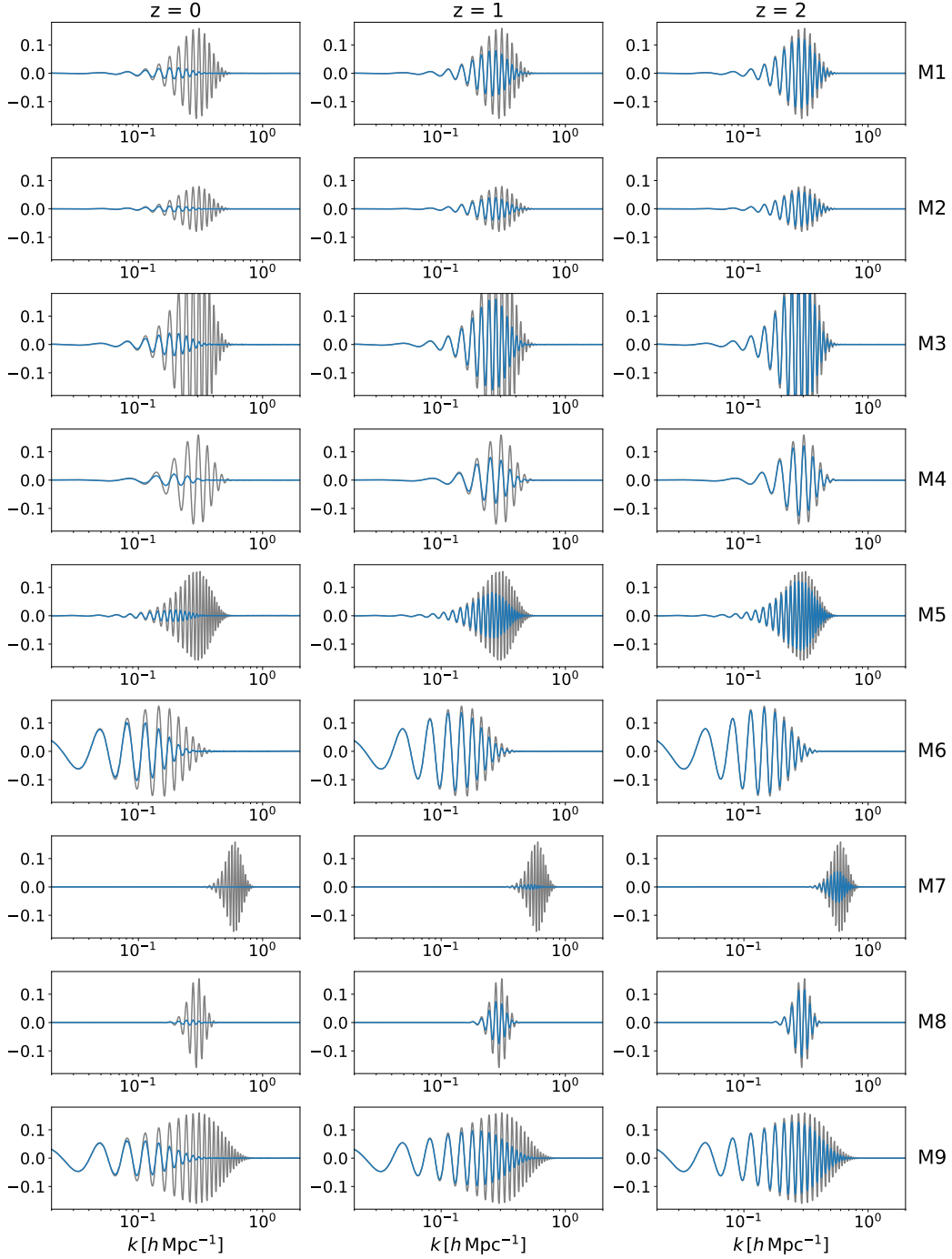


Figure 4. Relative differences with respect to the Λ CDM matter power spectrum for the linear matter power spectrum (gray) and the nonlinear matter power spectrum obtained from the simulations (blue) for the template with damped linear oscillations (2.1) at redshift $z = 0, 1, 2$.

and $k_* = 0.05 \text{ Mpc}^{-1}$. Here we have factored out the time-dependence given by the growth factor $G(z)$. The cross term in Eq. (4.2) is subdominant since it is proportional

to $A_{\text{BAO}} \cdot \mathcal{A}_{\text{lin}} \simeq 0.01$ and we neglect it.

The IR resummed power spectrum at leading order (LO) is given by

$$P^{\text{IR res, LO}}(z, k) = G^2(z) \left[P^{\text{nw}}(k) + e^{-k^2 G^2(z) \Sigma^2} P^{\text{w}}(k) \right] \quad (4.4)$$

where $P^{\text{nw}}(k)$ corresponds to the smooth part of the linear power spectrum and $P^{\text{w}}(k)$ is multiplied by the exponential damping of the oscillatory part due to the effect of IR enhanced loop contributions, exactly as for BAO [51]. For BAO, the damping factor corresponds to

$$\Sigma_{\text{BAO}}^2(k_{\text{S}}) \equiv \int_0^{k_{\text{S}}} \frac{dq}{6\pi^2} P^{\text{nw}}(q) [1 - j_0(qr_{\text{s}}) + 2j_2(qr_{\text{s}})] \quad (4.5)$$

where j_n are spherical Bessel functions and k_{S} is the separation scale of long and short modes, that has been introduced in order to treat the perturbative expansion in the two regimes separately. The dependence of the spectrum from k_{S} can be connected with an estimate of the perturbative uncertainty. For this reason and since IR expansions are valid for $q \ll k$, we assumed $k_{\text{S}} = \epsilon k$ with $\epsilon \in [0.3, 0.7]$ as in Ref. [32]. $r_{\text{s}} \simeq 147$ Mpc is the scale setting the period of the BAO [3]. For the primordial feature, the damping factor (4.5) depends also from the frequency ω_{lin} as

$$\Sigma_{\text{lin}}^2(\omega_{\text{lin}}, k_{\text{S}}) \equiv \int_0^{k_{\text{S}}} \frac{dq}{6\pi^2} P^{\text{nw}}(q) \left[1 - j_0\left(q \frac{\omega_{\text{lin}}}{k_*}\right) + 2j_2\left(q \frac{\omega_{\text{lin}}}{k_*}\right) \right]. \quad (4.6)$$

We can rewrite Eq. (4.4) as

$$P^{\text{IR res, LO}}(z, k) = G^2(z) P^{\text{nw}}(k) \left[1 + e^{-k^2 G^2(z) \Sigma_{\text{BAO}}^2} \delta P_{\text{BAO}}^{\text{w}}(k) + e^{-k^2 G^2(z) \Sigma_{\text{lin}}^2} \delta P_{\text{lin}}^{\text{w}}(k) \right]. \quad (4.7)$$

At next-to-leading order (NLO), the IR resummed power spectrum can be written in the form

$$P^{\text{IR res, LO+NLO}}(z, k) = G^2(z) P^{\text{nw}}(k) \left\{ 1 + [1 + k^2 G^2(z) \Sigma_{\text{BAO}}^2] e^{-k^2 G^2(z) \Sigma_{\text{BAO}}^2} \delta P_{\text{BAO}}^{\text{w}}(k) + [1 + k^2 G^2(z) \Sigma_{\text{lin}}^2] e^{-k^2 G^2(z) \Sigma_{\text{lin}}^2} \delta P_{\text{lin}}^{\text{w}}(k) \right\} + G^4(z) P^{1\text{-loop}} [P^{\text{IR res, LO}}(k)] \quad (4.8)$$

where we neglected the leading contribution to the NLO coming from 2-loops being numerically small (see Ref. [51] for the full expression at NLO for the resummed featureless matter power spectrum). We also neglect contribution to the power spectrum coming from the bispectrum that might become relevant for higher frequency compared to the one studied here. $P^{1\text{-loop}}$ is the standard one-loop result, but computed with the LO IR resummed power spectrum. In practice, one can use the usual expression $P^{1\text{-loop}} = P_{22} + 2P_{13}$, however evaluating the loop integrals P_{22} and P_{13} with the input spectrum $P^{\text{IR res, LO}}$ instead of the linear spectrum [50]. Note that we do not consider for any correction due to the Gaussian envelop just considering the linear oscillatory pattern on top of the matter power spectrum as it happens for BAO [51].

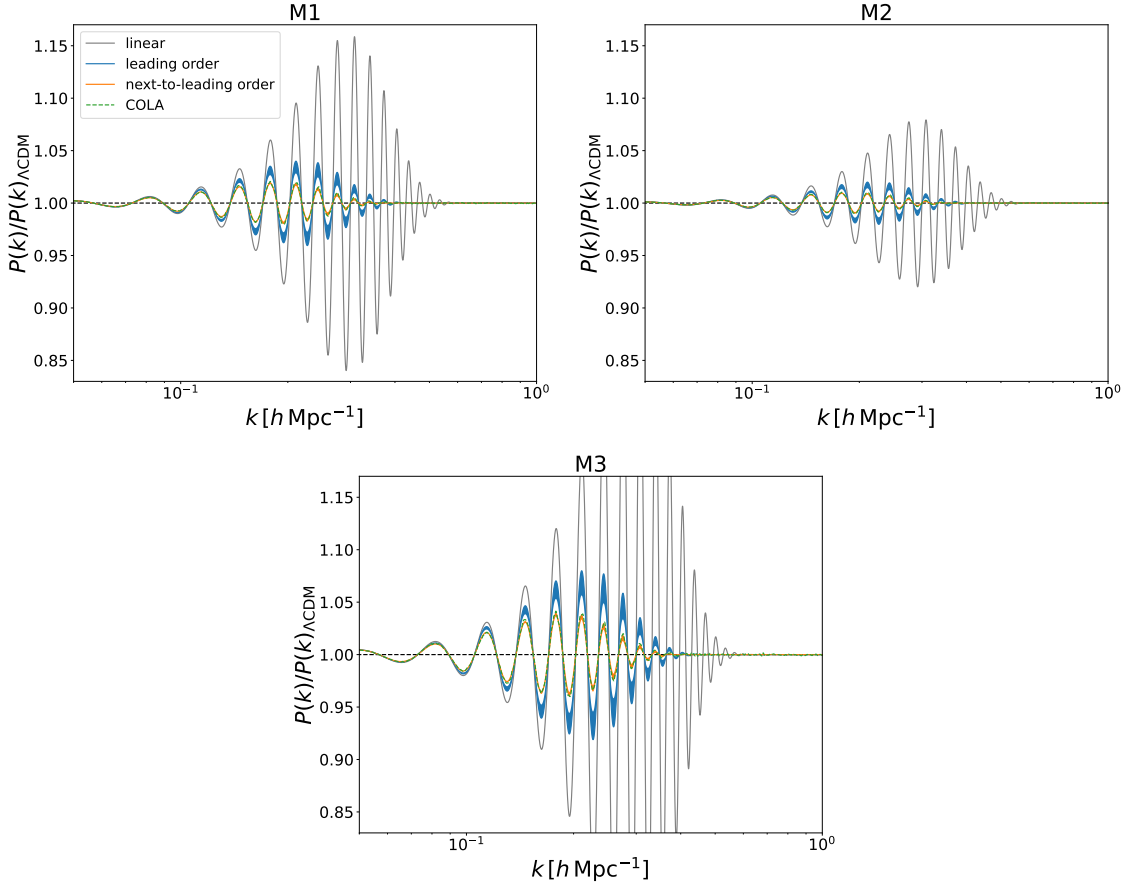


Figure 5. Ratio of IR resummed matter power spectrum at LO (blue) and NLO (orange) obtained for the damped linear oscillations to the one obtained with a power-law PPS at redshift $z = 0$ varying the IR separation scale $k_S = \epsilon k$ with $\epsilon \in [0.3, 0.7]$. Also shown is the linear result (gray). We show the results obtained from simulations (green dashed) for the best-fit parameters M1 (top left panel) and we change the value of the feature amplitude to $\mathcal{A}_{\text{lin}} = 0.08$ (top right panel) and $\mathcal{A}_{\text{lin}} = 0.32$ (bottom panel).

4.1 Comparison with cosmological simulations

In Figs. 5-6-7-8, we show the ratio between the matter power spectrum with damped primordial oscillations and the one with power-law PPS calculated at redshift $z = 0$ for the results both at LO and NLO. In particular, we vary the amplitude \mathcal{A}_{lin} in Fig. 5, the mean of the Gaussian envelope μ_{env} in Fig. 6, the dispersion of the Gaussian envelope σ_{env} in Fig. 7, and the feature frequency $\log_{10} \omega_{\text{lin}}$ in Fig. 8.

One can observe that the agreement between simulations and perturbation theory predictions is considerably improved going from LO to NLO. Furthermore, the dependence on the separation scale k_S is reduced (reducing the theoretical perturbative uncertainties). We find for the Fourier matter power spectrum at $z = 0$ differences less than 3% for the LO and less than 0.3% including the NLO with respect to our DM-only simulations, see Fig. 9. These differences and the predictions from perturba-

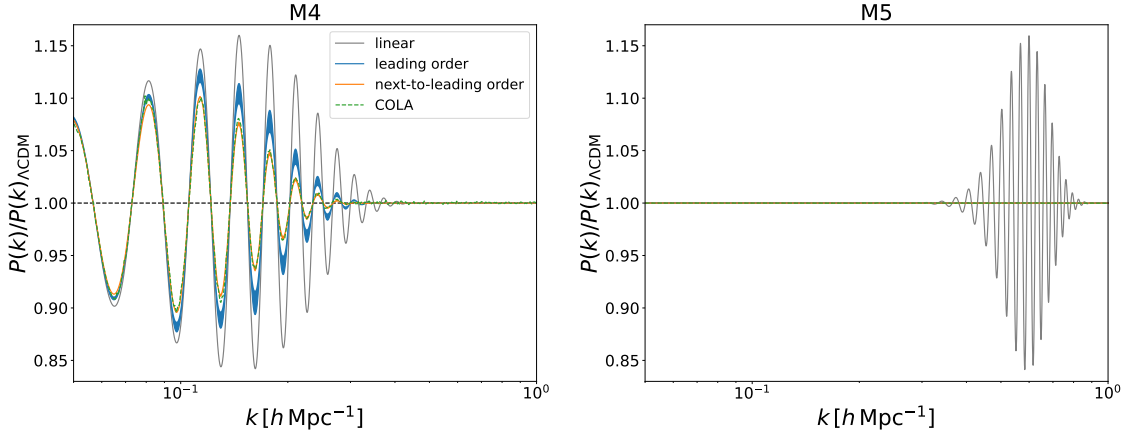


Figure 6. As Fig. 5 for $\mu_{\text{env}} = 0.1 \text{ Mpc}^{-1}$ (left panel) and for $\mu_{\text{env}} = 0.4 \text{ Mpc}^{-1}$ (right panel).

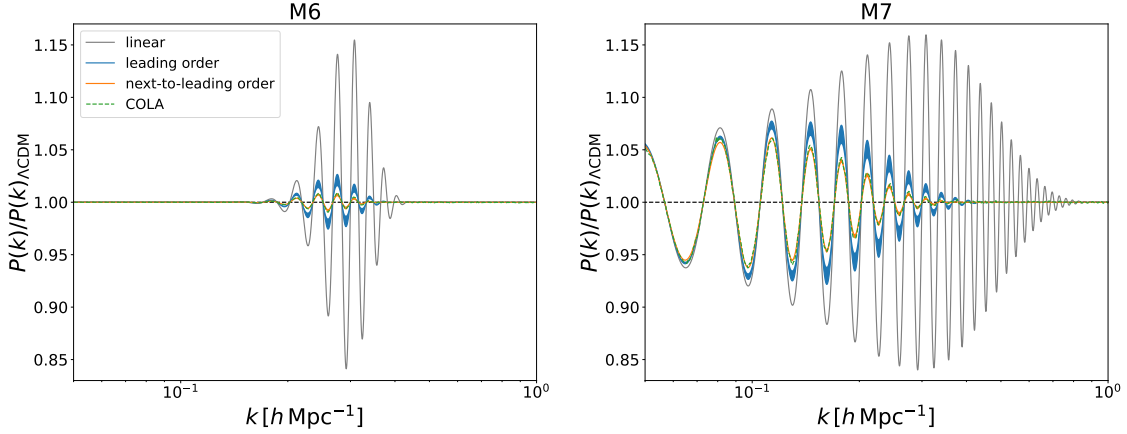


Figure 7. As Fig. 5 for $\sigma_{\text{env}} = 0.0285 \text{ Mpc}^{-1}$ (left panel) and for $\sigma_{\text{env}} = 0.114 \text{ Mpc}^{-1}$ (right panel).

tion theory are robust to the variation of the primordial feature parameters \mathcal{A}_{lin} , μ_{env} , σ_{env} , and $\log_{10} \omega_{\text{lin}}$.

Moving the position of the feature toward smaller scales, i.e. $\mu_{\text{env}} > 0.2 \text{ Mpc}^{-1}$, we see that the primordial oscillations are completely damped at low redshift, see Figs. 4-6. Analogously when we reduce the size of the Gaussian envelope, i.e. $\sigma_{\text{env}} < 0.057 \text{ Mpc}^{-1}$, see Figs. 4-7.

For the best-fit parameters M1, the amplitude of the oscillations is reduced by a factor 8 at $z = 0$ and it is reduced by half at $z = 1$. This effect is increased or reduced by varying the parameters of the Gaussian envelope with respect to their fiducial values. Moreover, all the primordial oscillations at $k > 0.3 \text{ h Mpc}^{-1}$ and $z = 0$ are washed away by nonlinearities. This result highlight the importance and the need of high redshift clustering measurements, i.e. $z \gtrsim 1$, in order to study these specific features on the matter power spectrum.

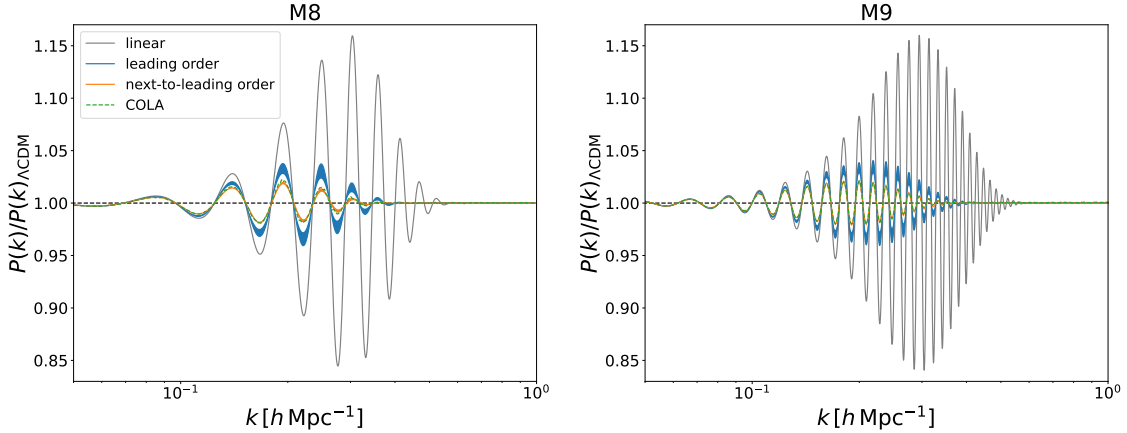


Figure 8. As Fig. 5 for $\log_{10} \omega_{\text{lin}} = 0.926$ (top panel) and for $\log_{10} \omega_{\text{lin}} = 1.39$ (bottom panel).

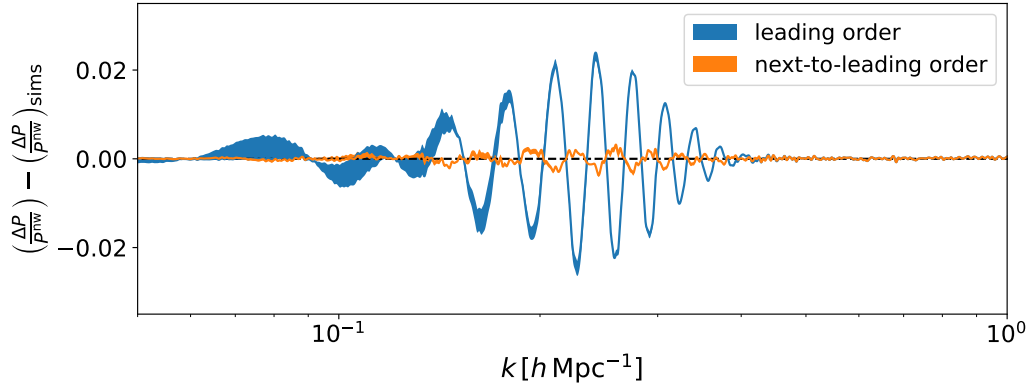


Figure 9. Comparison of the primordial oscillatory component of the matter power spectrum as predicted by LO (blue) and NLO (orange) with respect to the result from N-body simulations varying the IR separation scale $k_S = \epsilon k$ with $\epsilon \in [0.3, 0.7]$.

5 Comparison with current LSS data

We apply the methodology developed in Ref. [30] and already applied to the case of linear undamped oscillations to the current model with the publicly available library `CosmoBolognaLib`⁵ [52]. We consider the combination of two non-overlapping redshift bins, neglecting their correlation, covering $0.2 < z < 0.5$ and $0.5 < z < 0.75$ using the galaxy two-point correlation function (2PCF) from the Sloan Digital Sky Survey III Baryon Oscillation Spectroscopic Survey Data Release 12 (BOSS DR12) [53, 54].

The templates for the anisotropic 2PCF monopole and quadrupole are built start-

⁵<https://gitlab.com/federicomarulli/CosmoBolognaLib>

ing from the non-linear galaxy power spectrum in redshift space [55–58]

$$P(z, k, \mu) = \left[\frac{1 + \beta \mu^2 R(k, \Sigma_r)}{1 + k^2 \mu^2 \Sigma_s^2 / 2} \right]^2 P^{\text{IRres, LO}}(z, k, \mu). \quad (5.1)$$

Following the BOSS DR12 2PCF analysis [54], we fix the streaming scale at $\Sigma_s = 4 h^{-1}$ Mpc, the radial and transverse components of the standard Gaussian damping of BAO at $\Sigma_{\parallel} = 4 h^{-1}$ Mpc, and $\Sigma_{\perp} = 2.5 h^{-1}$ Mpc for post-reconstruction results, where $\Sigma_{\text{BAO}}^2 = \mu^2 \Sigma_{\parallel}^2 + (1 - \mu^2) \Sigma_{\perp}^2$. $R(k, \Sigma_r) = 1 - e^{-k^2 \Sigma_r^2 / 2}$ is the smoothing applied in reconstruction and $\Sigma_r = 15 h^{-1}$ Mpc is the smoothing scale used when deriving the displacement field [59]. Given Eq. (5.1), we define the multipole moments

$$P_{\ell}(k, \mu) = \frac{2\ell + 1}{2} \int_{-1}^{+1} d\mu P(k, \mu) L_{\ell}(\mu) \quad (5.2)$$

where $L_{\ell}(\mu)$ are Legendre polynomials. These are transformed to 2PCF multipole

$$\xi_{\ell}(s) = \frac{i^{\ell}}{2\pi^2} \int dk k^2 P_{\ell}(k, \mu) j_{\ell}(ks) \quad (5.3)$$

where $j_{\ell}(ks)$ is the ℓ -th order spherical Bessel function. We then use

$$\xi(s, \mu) = \sum_{\ell=0,2} \xi_{\ell}(s) L_{\ell}(\mu), \quad (5.4)$$

and we take averages over μ window to create the template

$$\xi_{\ell}(s, \alpha_{\perp}, \alpha_{\parallel}) = \int_{-1}^1 d\mu P_{\ell}(\mu') \xi(s', \mu') \quad (5.5)$$

where $\mu_{\text{true}} = \mu \alpha_{\parallel} / \sqrt{\mu^2 \alpha_{\parallel}^2 + (1 - \mu^2) \alpha_{\perp}^2}$, $s_{\text{true}} = s \sqrt{\mu^2 \alpha_{\parallel}^2 + (1 - \mu^2) \alpha_{\perp}^2}$. Finally, we fit to the data using the following model for the monopole and quadrupole of the 2PCF

$$\xi_0(s) = B_0 \xi_0(s, \alpha_{\perp}, \alpha_{\parallel}) + A_0^0 + \frac{A_0^1}{s} + \frac{A_0^2}{s^2}, \quad (5.6)$$

$$\xi_2(s) = \frac{5}{2} [B_2 \xi_2(s, \alpha_{\perp}, \alpha_{\parallel}) - B_0 \xi_0(s, \alpha_{\perp}, \alpha_{\parallel})] + A_2^0 + \frac{A_2^1}{s} + \frac{A_2^2}{s^2}. \quad (5.7)$$

We vary the amplitude of the template (2.1) (linearly in the range $\mathcal{A}_{\text{lin}} \in [0, 1]$) together with the BAO ($\alpha_{\perp}, \alpha_{\parallel}$) and nuisance parameters ($B_0, B_2, A_0^0, A_0^2, A_1^0, A_1^2, A_2^0, A_2^2$) _{z_1, z_2} keeping fix the remaining four primordial feature parameters. B_0 and B_2 are used to marginalize over the power spectra amplitude, i.e. clustering bias amplitude and redshift-space distortions effects. All the A_j^i parameters are used to marginalize over the broad-band effects including angle-dependent overall shape of the power spectra, redshift space distortions, scale-dependent bias, and any errors made in our assumption of the model cosmology; see Ref. [54]. These nuisance parameters

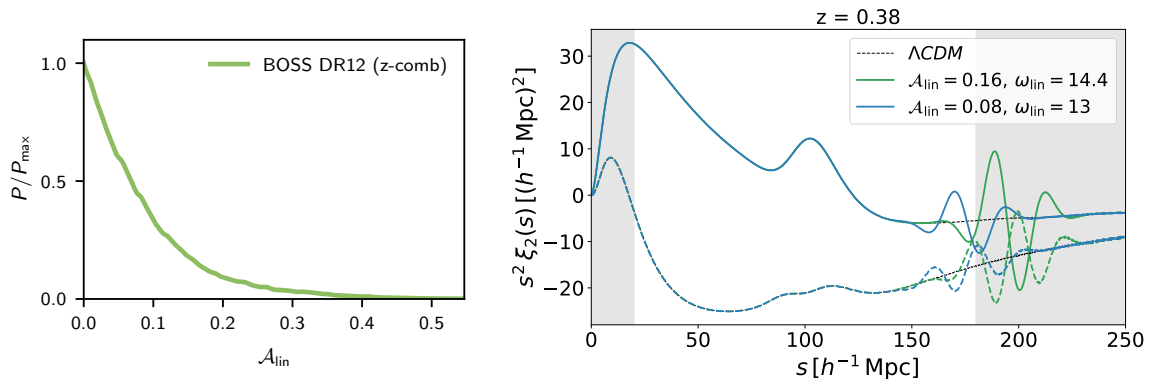


Figure 10. *Left panel:* marginalized posterior distribution of the amplitude of the feature obtained with the BOSS DR12 combined redshift bin. *Right panel:* nonlinear CDM 2PCF monopole (solid) and quadrupole (dashed) computed at $z = 0.38$ (central redshift of the first BOSS DR12 bin) for M1 (green) and a case with half amplitude $\mathcal{A}_{\text{lin}} = 0.08$ and lower frequency $\omega_{\text{lin}} = 13$ (blue). We highlight in gray the scales excluded in the analysis, i.e. $s < 20 h^{-1} \text{Mpc}$ and $s > 180 h^{-1} \text{Mpc}$. Black lines correspond to the monopole and quadrupole predictions of ΛCDM with power-law PPS.

cover also for the marginalization over effects due to the scale-dependent clustering bias contribution which is expected to be very small for primordial features; see [25, 60]. We find $\mathcal{A}_{\text{lin}} < 0.26$ (< 0.096) at 95% (68%) confidence level (CL), we show the marginalized poster distribution on \mathcal{A}_{lin} in Fig. 10.

The constraints are weaker compared to the one we found for the undamped linear oscillations in Ref. [30] because the best-fit frequency $\omega_{\text{lin}} \simeq 14.4$ is at very large separation scales of the 2PCF, mostly beyond the BOSS measurements, see Fig. 10. Indeed, for such frequency, the best-fit amplitude $\mathcal{A}_{\text{lin}} = 0.16$ is still allowed from BOSS DR12 galaxy correlation data; note however that BOSS DR12 2PCF [30] will probe more efficiently lower frequencies $\omega_{\text{lin}} \lesssim 13$. Tighter constraints could also be obtained by full-shape matter power spectrum data [27].

6 Conclusions

A primordial signal with an oscillatory pattern superimposed to the PPS can mimic the smoothing excess in the region of the acoustic peaks measured by *Planck* and quantified by the phenomenological parameter A_L .

It is important to stress that while it is possible to find a specific localized oscillation able to reproduce a signal close to the one generated by $A_L \simeq 1.18$ in CMB temperature power spectrum, we expect that this does not hold for CMB polarization [15]. Such a primordial localized oscillation can leave an imprint on the clustering of the galaxy distribution.

In this paper, we have accurately modelled the imprint of this specific localized oscillation on the matter power spectrum. We have run a set DM-only cosmological simulations varying some of the feature parameters of the template (2.1) at the time

with $1,024^3$ DM particles in a comoving box with side length of $1,024 h^{-1}$ Mpc consistently with Ref. [28]. We have compared then the nonlinear CDM power spectra with the prediction from perturbation theory [50, 51] showing a good agreement when the NLO is included, better than 0.3% for the envelope of the feature. The large amplitude of the feature, i.e. $\mathcal{A}_{\text{lin}} \simeq 0.16$, required to mimic the effect of $A_L \simeq 1.18$ on the CMB temperature angular power spectrum is strongly damped by nonlinearities. The amplitude of the feature is reduced approximately by a factor 8 at $z = 0$ and it is halved at $z = 1$.

Finally, we have derived the constraint on the amplitude keeping fixed the other feature parameters. We have followed the methodology developed in Ref. [30] to constrain feature templates with undamped oscillations and a localized bump with the BOSS DR12 galaxy 2PCF. Contrary to the tight constraint found in the case of undamped linear primordial oscillations in Ref. [30], i.e. $\mathcal{A}_{\text{lin}}^{\text{undamped}} < 0.025$ at 95% CL, we find a weaker upper bound for this specific template since the position of the localized wave packet of linearly spaced oscillations is at very small scales, around $k \sim 0.2 h/\text{Mpc}$, almost outside the observational window of the 2PCF, see Fig. 10. Here we find a constraint of $\mathcal{A}_{\text{lin}} < 0.26$ at 95% CL for $\omega_{\text{lin}} \simeq 14.4$.

Future galaxy clustering measurements at high redshift $z \gtrsim 1$ from Euclid [61] are the most sensitive to these primordial oscillations mimicking \mathcal{A}_L and will improve significantly the observational status presented here.

Acknowledgments

FF would like to thank Akhil Antony, Jan Hamann, Dhiraj Kumar Hazra, Arman Shafieloo, and Matteo Tagliacruz for discussions on the subject. MB and FF acknowledge financial support from the contract ASI/ INAF for the Euclid mission n.2018-23-HH.0 and from the ASI Grant 2016-24-H.0 and the agreement n. 2020-9-HH.0 ASI-UniRM2 “Partecipazione italiana alla fase A della missione LiteBIRD”.

References

- [1] P. A. R. Ade *et al.* [Planck], *Astron. Astrophys.* **571** (2014), A16
doi:10.1051/0004-6361/201321591 [arXiv:1303.5076 [astro-ph.CO]].
- [2] P. A. R. Ade *et al.* [Planck], *Astron. Astrophys.* **594** (2016), A13
doi:10.1051/0004-6361/201525830 [arXiv:1502.01589 [astro-ph.CO]].
- [3] N. Aghanim *et al.* [Planck], *Astron. Astrophys.* **641** (2020), A6 [erratum: *Astron. Astrophys.* **652** (2021), C4] doi:10.1051/0004-6361/201833910 [arXiv:1807.06209 [astro-ph.CO]].
- [4] W. Handley, *Phys. Rev. D* **103** (2021) no.4, L041301
doi:10.1103/PhysRevD.103.L041301 [arXiv:1908.09139 [astro-ph.CO]].
- [5] E. Di Valentino, A. Melchiorri and J. Silk, *Nature Astron.* **4** (2019) no.2, 196-203
doi:10.1038/s41550-019-0906-9 [arXiv:1911.02087 [astro-ph.CO]].

- [6] G. Efstathiou and S. Gratton, *Mon. Not. Roy. Astron. Soc.* **496** (2020) no.1, L91-L95 doi:10.1093/mnrasl/slaa093 [arXiv:2002.06892 [astro-ph.CO]].
- [7] N. Aghanim *et al.* [Planck], *Astron. Astrophys.* **641** (2020), A5 doi:10.1051/0004-6361/201936386 [arXiv:1907.12875 [astro-ph.CO]].
- [8] G. Efstathiou and S. Gratton, doi:10.21105/astro.1910.00483 [arXiv:1910.00483 [astro-ph.CO]].
- [9] E. Calabrese, A. Slosar, A. Melchiorri, G. F. Smoot and O. Zahn, *Phys. Rev. D* **77** (2008), 123531 doi:10.1103/PhysRevD.77.123531 [arXiv:0803.2309 [astro-ph]].
- [10] E. Rosenberg, S. Gratton and G. Efstathiou, [arXiv:2205.10869 [astro-ph.CO]].
- [11] S. Aiola *et al.* [ACT], *JCAP* **12** (2020), 047 doi:10.1088/1475-7516/2020/12/047 [arXiv:2007.07288 [astro-ph.CO]].
- [12] D. Dutcher *et al.* [SPT-3G], *Phys. Rev. D* **104** (2021) no.2, 022003 doi:10.1103/PhysRevD.104.022003 [arXiv:2101.01684 [astro-ph.CO]].
- [13] N. Aghanim *et al.* [Planck], *Astron. Astrophys.* **641** (2020), A8 doi:10.1051/0004-6361/201833886 [arXiv:1807.06210 [astro-ph.CO]].
- [14] G. Domènech and M. Kamionkowski, *JCAP* **11** (2019), 040 doi:10.1088/1475-7516/2019/11/040 [arXiv:1905.04323 [astro-ph.CO]].
- [15] Y. Akrami *et al.* [Planck], *Astron. Astrophys.* **641** (2020), A10 doi:10.1051/0004-6361/201833887 [arXiv:1807.06211 [astro-ph.CO]].
- [16] G. Domènech, X. Chen, M. Kamionkowski and A. Loeb, *JCAP* **10** (2020), 005 doi:10.1088/1475-7516/2020/10/005 [arXiv:2005.08998 [astro-ph.CO]].
- [17] D. K. Hazra, A. Antony and A. Shafieloo, *JCAP* **08** (2022) no.08, 063 doi:10.1088/1475-7516/2022/08/063 [arXiv:2201.12000 [astro-ph.CO]].
- [18] A. Antony, F. Finelli, D. K. Hazra and A. Shafieloo, [arXiv:2202.14028 [astro-ph.CO]].
- [19] D. K. Hazra, A. Shafieloo and T. Souradeep, *JCAP* **11** (2014), 011 doi:10.1088/1475-7516/2014/11/011 [arXiv:1406.4827 [astro-ph.CO]].
- [20] D. J. Eisenstein and W. Hu, *Astrophys. J.* **496** (1998), 605 doi:10.1086/305424 [arXiv:astro-ph/9709112 [astro-ph]].
- [21] Z. Huang, L. Verde and F. Vernizzi, *JCAP* **04** (2012), 005 doi:10.1088/1475-7516/2012/04/005 [arXiv:1201.5955 [astro-ph.CO]].
- [22] X. Chen, P. D. Meerburg and M. Münchmeyer, *JCAP* **09** (2016), 023 doi:10.1088/1475-7516/2016/09/023 [arXiv:1605.09364 [astro-ph.CO]].
- [23] X. Chen, C. Dvorkin, Z. Huang, M. H. Namjoo and L. Verde, *JCAP* **11** (2016), 014 doi:10.1088/1475-7516/2016/11/014 [arXiv:1605.09365 [astro-ph.CO]].
- [24] M. Ballardini, F. Finelli, C. Fedeli and L. Moscardini, *JCAP* **10** (2016), 041 [erratum: *JCAP* **04** (2018), E01] doi:10.1088/1475-7516/2016/10/041 [arXiv:1606.03747 [astro-ph.CO]].
- [25] M. Ballardini, F. Finelli, R. Maartens and L. Moscardini, *JCAP* **04** (2018), 044 doi:10.1088/1475-7516/2018/04/044 [arXiv:1712.07425 [astro-ph.CO]].

- [26] A. Slosar, K. N. Abazajian, M. Abidi, P. Adshead, Z. Ahmed, D. Alonso, M. A. Amin, B. Ansarinejad, R. Armstrong and C. Baccigalupi, *et al.* *Bull. Am. Astron. Soc.* **51** (2019) no.3, 98 [arXiv:1903.09883 [astro-ph.CO]].
- [27] F. Beutler, M. Biagetti, D. Green, A. Slosar and B. Wallisch, *Phys. Rev. Res.* **1** (2019) no.3, 033209 doi:10.1103/PhysRevResearch.1.033209 [arXiv:1906.08758 [astro-ph.CO]].
- [28] M. Ballardini, R. Murgia, M. Baldi, F. Finelli and M. Viel, *JCAP* **04** (2020) no.04, 030 doi:10.1088/1475-7516/2020/04/030 [arXiv:1912.12499 [astro-ph.CO]].
- [29] C. Zeng, E. D. Kovetz, X. Chen, Y. Gong, J. B. Muñoz and M. Kamionkowski, *Phys. Rev. D* **99** (2019) no.4, 043517 doi:10.1103/PhysRevD.99.043517 [arXiv:1812.05105 [astro-ph.CO]].
- [30] M. Ballardini, F. Finelli, F. Marulli, L. Moscardini and A. Veropalumbo, [arXiv:2202.08819 [astro-ph.CO]].
- [31] Z. Vlah, U. Seljak, M. Y. Chu and Y. Feng, *JCAP* **03** (2016), 057 doi:10.1088/1475-7516/2016/03/057 [arXiv:1509.02120 [astro-ph.CO]].
- [32] A. Vasudevan, M. M. Ivanov, S. Sibiryakov and J. Lesgourgues, *JCAP* **09** (2019), 037 doi:10.1088/1475-7516/2019/09/037 [arXiv:1906.08697 [astro-ph.CO]].
- [33] S. F. Chen, Z. Vlah and M. White, *JCAP* **11** (2020), 035 doi:10.1088/1475-7516/2020/11/035 [arXiv:2007.00704 [astro-ph.CO]].
- [34] Y. Li, H. M. Zhu and B. Li, *Mon. Not. Roy. Astron. Soc.* **514** (2022), 4363 doi:10.1093/mnras/stac1544 [arXiv:2102.09007 [astro-ph.CO]].
- [35] M. A. Troxel *et al.* [DES], *Phys. Rev. D* **98** (2018) no.4, 043528 doi:10.1103/PhysRevD.98.043528 [arXiv:1708.01538 [astro-ph.CO]].
- [36] B. A. Reid, W. J. Percival, D. J. Eisenstein, L. Verde, D. N. Spergel, R. A. Skibba, N. A. Bahcall, T. Budavari, M. Fukugita and J. R. Gott, *et al.* *Mon. Not. Roy. Astron. Soc.* **404** (2010), 60-85 doi:10.1111/j.1365-2966.2010.16276.x [arXiv:0907.1659 [astro-ph.CO]].
- [37] B. Abolfathi *et al.* [SDSS], *Astrophys. J. Suppl.* **235** (2018) no.2, 42 doi:10.3847/1538-4365/aa9e8a [arXiv:1707.09322 [astro-ph.GA]].
- [38] S. Chabanier, M. Millea and N. Palanque-Delabrouille, *Mon. Not. Roy. Astron. Soc.* **489** (2019) no.2, 2247-2253 doi:10.1093/mnras/stz2310 [arXiv:1905.08103 [astro-ph.CO]].
- [39] M. Tegmark and M. Zaldarriaga, *Phys. Rev. D* **66** (2002), 103508 doi:10.1103/PhysRevD.66.103508 [arXiv:astro-ph/0207047 [astro-ph]].
- [40] R. S. Chandra and T. Souradeep, *JCAP* **10** (2021), 081 doi:10.1088/1475-7516/2021/10/081 [arXiv:2104.12253 [astro-ph.CO]].
- [41] S. Tassev, M. Zaldarriaga and D. Eisenstein, *JCAP* **06** (2013), 036 doi:10.1088/1475-7516/2013/06/036 [arXiv:1301.0322 [astro-ph.CO]].
- [42] C. Howlett, M. Manera and W. J. Percival, *Astron. Comput.* **12** (2015), 109-126 doi:10.1016/j.ascom.2015.07.003 [arXiv:1506.03737 [astro-ph.CO]].

- [43] H. A. Winther, K. Koyama, M. Manera, B. S. Wright and G. B. Zhao, *JCAP* **08** (2017), 006 doi:10.1088/1475-7516/2017/08/006 [arXiv:1703.00879 [astro-ph.CO]].
- [44] M. Crocce, S. Pueblas and R. Scoccimarro, *Mon. Not. Roy. Astron. Soc.* **373** (2006), 369-381 doi:10.1111/j.1365-2966.2006.11040.x [arXiv:astro-ph/0606505 [astro-ph]].
- [45] A. Lewis, A. Challinor and A. Lasenby, *Astrophys. J.* **538** (2000), 473-476 doi:10.1086/309179 [arXiv:astro-ph/9911177 [astro-ph]].
- [46] M. Viel, M. G. Haehnelt and V. Springel, *JCAP* **06** (2010), 015 doi:10.1088/1475-7516/2010/06/015 [arXiv:1003.2422 [astro-ph.CO]].
- [47] A. Pontzen, A. Slosar, N. Roth and H. V. Peiris, *Phys. Rev. D* **93** (2016) no.10, 103519 doi:10.1103/PhysRevD.93.103519 [arXiv:1511.04090 [astro-ph.CO]].
- [48] R. E. Angulo and A. Pontzen, *Mon. Not. Roy. Astron. Soc.* **462** (2016) no.1, L1-L5 doi:10.1093/mnras/slw098 [arXiv:1603.05253 [astro-ph.CO]].
- [49] F. Villaescusa-Navarro, S. Naess, S. Genel, A. Pontzen, B. Wandelt, L. Anderson, A. Font-Ribera, N. Battaglia and D. N. Spergel, *Astrophys. J.* **867** (2018) no.2, 137 doi:10.3847/1538-4357/aae52b [arXiv:1806.01871 [astro-ph.CO]].
- [50] D. Blas, M. Garny, M. M. Ivanov and S. Sibiryakov, *JCAP* **07** (2016), 052 doi:10.1088/1475-7516/2016/07/052 [arXiv:1512.05807 [astro-ph.CO]].
- [51] D. Blas, M. Garny, M. M. Ivanov and S. Sibiryakov, *JCAP* **07** (2016), 028 doi:10.1088/1475-7516/2016/07/028 [arXiv:1605.02149 [astro-ph.CO]].
- [52] F. Marulli, A. Veropalumbo and M. Moresco, *Astron. Comput.* **14** (2016), 35-42 doi:10.1016/j.ascom.2016.01.005 [arXiv:1511.00012 [astro-ph.CO]].
- [53] S. Alam *et al.* [BOSS], *Mon. Not. Roy. Astron. Soc.* **470** (2017) no.3, 2617-2652 doi:10.1093/mnras/stx721 [arXiv:1607.03155 [astro-ph.CO]].
- [54] A. J. Ross *et al.* [BOSS], *Mon. Not. Roy. Astron. Soc.* **464** (2017) no.1, 1168-1191 doi:10.1093/mnras/stw2372 [arXiv:1607.03145 [astro-ph.CO]].
- [55] N. Kaiser, *Mon. Not. Roy. Astron. Soc.* **227** (1987), 1-27
- [56] K. B. Fisher, C. A. Scharf and O. Lahav, *Mon. Not. Roy. Astron. Soc.* **266** (1994), 219-226 doi:10.1093/mnras/266.1.219 [arXiv:astro-ph/9309027 [astro-ph]].
- [57] X. Xu, N. Padmanabhan, D. J. Eisenstein, K. T. Mehta and A. J. Cuesta, *Mon. Not. Roy. Astron. Soc.* **427** (2012), 2146 doi:10.1111/j.1365-2966.2012.21573.x [arXiv:1202.0091 [astro-ph.CO]].
- [58] X. Xu, A. J. Cuesta, N. Padmanabhan, D. J. Eisenstein and C. K. McBride, *Mon. Not. Roy. Astron. Soc.* **431** (2013), 2834 doi:10.1093/mnras/stt379 [arXiv:1206.6732 [astro-ph.CO]].
- [59] H. J. Seo, F. Beutler, A. J. Ross and S. Saito, *Mon. Not. Roy. Astron. Soc.* **460** (2016) no.3, 2453-2471 doi:10.1093/mnras/stw1138 [arXiv:1511.00663 [astro-ph.CO]].
- [60] G. Cabass, E. Pajer and F. Schmidt, *JCAP* **09** (2018), 003 doi:10.1088/1475-7516/2018/09/003 [arXiv:1804.07295 [astro-ph.CO]].
- [61] R. Laureijs *et al.* [EUCLID], [arXiv:1110.3193 [astro-ph.CO]].